ChemComm

Accepted Manuscript

This article can be cited before page numbers have been issued, to do this please use: P. Ling, C. Qian, F. Gao and J. Lei, *Chem. Commun.*, 2018, DOI: 10.1039/C8CC05068F.




ROYAL SOCIETY OF CHEMISTRY

rsc.li/chemcomm

View Article Online
DOI: 10.1039/C8CC05068F

ChemComm

COMMUNICATION

# Enzyme-immobilized metal-organic framework nanosheets as tandem catalysts for generation of nitric oxide†

Received 00th January 20xx,
Accepted 00th January 20xx

DOI: 10.XXXX/x0xx00000x

www.rsc.org/

Pinghua Ling,[a]* Caihua Qian,[a] Feng Gao[a] and Jianping Lei[b]*

**An enzyme-immobilized metal-organic framework (MOF) nanosheet system was developed as a tandem catalyst, which converted glucose into glucose acid and $H_2O_2$, and sequentially the latter could catalyze the oxidation of L-arginine to generate nitric oxide in the presence of porphyrinic MOF as artificial enzyme under physiological pH, showing great potential in cancer starving-like/gas therapy.**

Nitric oxide (NO) as a star molecule is an important endogenous signaling molecule and plays a pivotal role in physiological and pathological processes.[1] Recently, NO has been used in the field of cancer therapy. Furthermore, high NO content not only kills the cancerous cell but also could enhance the efficacy of therapy.[2] Inversely, low NO content may probably promote the progression of disease.[3] So it is necessary to develop activatable NO donors for the sustained NO release. L-Arginine (L-Arg) is a natural NO donor and can continuously release NO in the presence of inducible NO synthase (iNOS).[4] Previous studies also indicate $H_2O_2$ could oxidize L-Arg to NO.[5] It is expected that L-Arg in the $H_2O_2$-rich tumor cells could generate a large amount of NO. Thus, combining the NO-releasing materials and NO-generating catalysts with biomimic capacity is a possible solution to form NO.

The artificial enzymes or biomimetic systems have been studied for decades,[6] including iron oxide,[7] gold,[8] copper[9] nanoparticles, $Cu^{2+}$-modified carbon dots, carbon nitride nanoparticles or graphene oxide nanoparticles[10] and prussian blue nanoparticles.[11] Due to their unique characteristics relative to natural enzymes, artificial enzymes have been extensively explored for different applications, such as in bioanalysis,[12] molecular delivery,[13] bioimaging,[14] and biomedicine.[15] In contrast, the biological systems are complex chemical transformations rather than conventional chemical reactions under mild conditions, such as physiological pH, atmospheric pressure and aqueous solution. The processes are powered by a lot of reaction cascades facilitated by the synergistic protein catalysts via complex metabolic pathways. Studies have shown that coupling enzymatic catalysts and molecular catalysts or nanomaterials could construct tandem catalytic systems.[16] So, it is interesting in designing a synergistic reaction system with enzymatic catalysts and nanomaterials to use under physiological pH and room temperature conditions.

Immobilizing the enzyme on the common platform support can offer a plausible pathway. Recently, many conventional solid, such as zeolites, and mesoporous silica,[17] have been investigated to immobilize enzymes. Nevertheless, the lack of specific interactions between these materials and enzymes molecules results in loss of activity upon reuse.[17a,17b,18] Metal–organic frameworks (MOFs), a new class porous material, have been reported as enzyme mimetics or as a support for enzyme immobilization.[19] 2D MOFs, a newly developed material and a new member of the 2D material family, have received great attention.[20] Compared to traditional 3D bulk MOFs, 2D MOFs possess some advantages including large surface area, more accessible active sites on their surfaces and thickness of sub-10 nm.[20b,20c] 2D MOFs have been reported in versatile applications, such as catalysis,[20c,21] sensing,[22] gas separation.[20a,20b] Inspired by the unique physical and chemical properties of 2D MOFs, more and more attentions have been paid to synthesize and explore the function of 2D MOFs. Herein, 2D MOFs, Co-TCPP(Fe) nanosheets (Co-FeMOF) were chosen as both enzymatic mimic to catalyze the oxidation reaction and a support for enzyme immobilization to establish a tandem catalysts system.

FeTCPP, an iron porphyrin species, could catalyze the oxidation reaction of L-Arg by $H_2O_2$ to form citrulline and NO.[5b] However, it generally undergoes molecular aggregation and oxidative destruction, so it limits its application in many fields. Hydrophilic iron porphyrin derivatives immobilized on the resin could be used for the oxidation of L-Arg, but the system needs a high concentration of $H_2O_2$.[5c] In order to achieve the artificial enzyme system for tandem catalysis and local generation of NO, we immobilized glucose oxidase (GOD) on the surface of Co-FeMOF which was prepared by Co as node and FeTCPP as linker (Scheme 1). Glucose could be oxidized into glucose acid and $H_2O_2$ by GOD. On

[a] Laboratory of Functionalized Molecular Solids, Ministry of Education, Anhui Key Laboratory of Chemo/Biosensing, Laboratory of Optical Probes and Bioelectrocatalysis (LOPAB), College of Chemistry and Materials Science, Anhui Normal University, Wuhu 241002, P. R. China. E-mail: phling@ahnu.edu.cn.
[b] State Key Laboratory of Analytical Chemistry for Life Science, School of Chemistry and Chemical Engineering, Nanjing University, Nanjing 210023, P.R. China. E-mail: jpl@nju.edu.cn.

†Electronic Supplementary Information (ESI) available: Materials, methods, characterization and supplementary data. See DOI: 10.1039/b000000x/

View Article Online
DOI: 10.1039/C8CC05068F




the other hand, FeTCPP could catalyze the oxidation reaction of L-Arg for generation of NO. The strategy is expected to produce $H_2O_2$ locally from endogenous glucose for the subsequent Co-FeMOF catalytic oxidation of L-Arg to generate NO species.

In this way, this complex conjugate can be as a tandem catalyst to enable the continuous generation of NO from physiologically abundant glucose and L-Arg, and demonstrate that the artificial enzyme system can be mixed with serum to generate NO. The tandem catalysis, GOD@Co-FeMOF, has a great potential in the cancer starving-like/gas therapy.

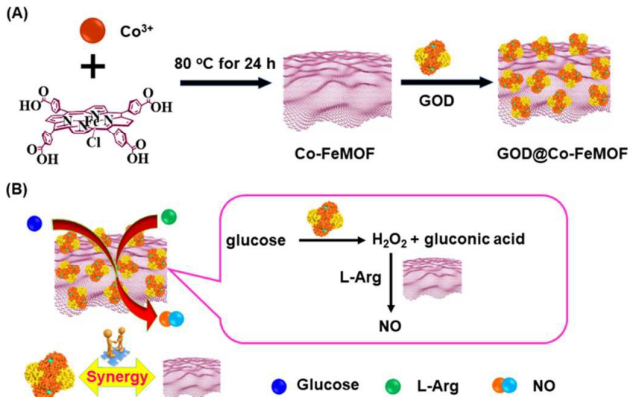


**Scheme 1** Schematic illustration of (A) preparation of GOD@Co-FeMOF composite and (B) the tandem catalysis strategy of toward L-Arg oxidation to produce NO.

In this work, the 2D MOFs, Co-FeMOF, was synthesized with Co as node and FeTCPP as linker. Powder X-ray diffraction (PXRD) was employed to investigate the polycrystalline feature of Co-FeMOF (Fig. 1A). The result depicts that the peaks at 7.6°, 8.8°, and 17°, which were indexed as (110), (002), and (004), respectively, indicating the successful assembly of Co-FeMOF.[20c,21] The morphology of Co-FeMOF was characterized by the scanning electron microscopy (SEM), selected area electron diffraction pattern (SAED) and transmission electron microscopy (TEM). The SEM result reveals the Co-FeMOF with sheet-like morphology and hundreds of nanometers (Fig. 1B). TEM image and SAED (Fig. 1C) show a well-dispersed and well-defined ultrathin sheet-like structures and polycrystalline nature. Compared with Co-FeMOF, the surface of GOD@Co-FeMOF displays some agglomerates on the surface (Fig. 1D), indicating the GOD was loaded on the surface of Co-FeMOF. Simultaneously, 1.0 mg/mL Co-FeMOF is optically equivalent to 0.25 mg/mL free FeTCPP (Fig. S1). According to the reduced mass in Fe element, the GOD content is determined to be 24% in the GOD@Co-FeMOF (Table S1 and S2).

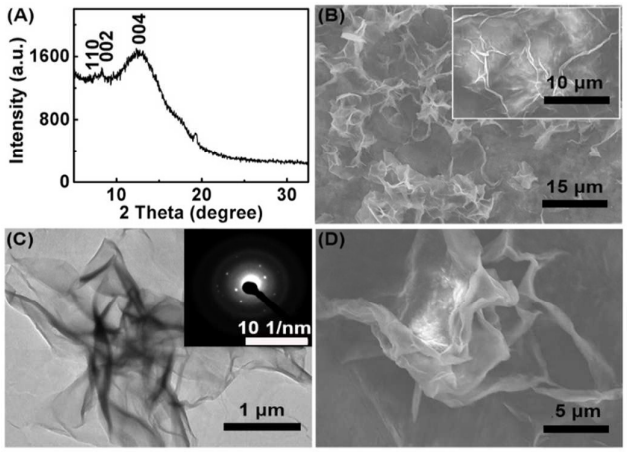


**Fig. 1** (A) Powder X-ray diffraction patterns, (B) SEM, and (C) TEM images of Co-FeMOF. Inset: SAED pattern. (D) SEM image of GOD@Co-FeMOF.

In order to further investigate the functionalization of Co-FeMOF with GOD, the UV-vis absorption spectra and the zeta potential were employed. As shown in Fig. S2A, the maximum absorption of GOD at 278 nm (curve a), which is the characteristic peak of GOD (Fig. S3). Compared with FeTCPP (curve b), the maximum Soret absorption of Co-FeMOF (curve c) shifts from 412 nm to ~427 nm, which maybe contribute to the hydrophobic nature of the octahedral cavity and the sensitivity of the Soret band to the dielectric constant of the solvent.[23] From the UV-vis absorption spectrum of GOD@Co-FeMOF (curve d), a new Soret absorption appeared at 278 nm in comparison with that of pure Co-FeMOF, illustrating the successful loading of the GOD protein on the surface of Co-FeMOF. Zeta potentials were also investigated (Fig. S2B). The results show that Co-FeMOF has a more positive potential than FeTCPP, mainly due to the FeTCPP self-assembled into Co-FeMOF with $Co^{3+}$ and the uncoordinated carboxyl group on the surface of the Co-FeMOF. The zeta potential of GOD@Co-FeMOF is slightly more negative than that of Co-FeMOF, indicating the successful functionalization of Co-FeMOF with GOD.

To examine the catalytic oxidation characteristics of Co-FeMOF, L-Arg oxidation reactions were conducted by dispersing the FeTCPP, Co-FeMOF and GOD@Co-FeMOF in a pH 7.4 PBS buffer with 20 mM L-Arg, along with 5.0 mM $H_2O_2$ as the oxidant and the production was identified by NO probe, 3-amino,4-aminomethyl1-2′,7′-difluorescein, diacetate (DAF-FM DA). It has been documented that NO can react with DAF-FM DA to form benzotriazole derivative with fluorescence emission. The fluorescence (FL) spectra were monitored at different conditions (Fig. 2), and the intensity increase of the emission peak at 515 nm corresponded NO generation. As shown in Fig. 2A, DAF-FM DA was mixed with $H_2O_2$ (curve a), L-Arg (curve b), glucose (curve c), FeTCPP (curve d), Co-FeMOF (curve e) and GOD@Co-FeMOF (curve f), individually, the benzotriazole derivative demonstrated none curve peaking at 515 nm. When DAF-FM DA was allowed to react with the mixture L-Arg and $H_2O_2$, the emission profile was increased at 515 nm (curve g), indicating $H_2O_2$ can oxidize L-Arg to produce NO.[5,24] Meanwhile, upon incubation with the mixture of FeTCPP, L-Arg and $H_2O_2$ (curve h), the mixture of GOD@Co-FeMOF, L-Arg and $H_2O_2$ (curve i) and the mixture of Co-FeMOF, L-Arg and $H_2O_2$ (curve j) for 25 min, respectively, the DAF-FM DA demonstrated a significant curve peaking at 515 nm. Furthermore, with the equivalent amount of FeTCPP, the Co-FeMOF catalysts show a higher activity, which could be attributed to FeTCPP with the monomeric molecular structure in Co-FeMOF. In order to verify the catalysis is derived from FeTCPP, the FL of Co-MOF which is prepared with Co and TCPP (nonmetallic porphyrin)

View Article Online
DOI: 10.1039/C8CC05068F





mixed with 20 mM L-Arg, 5.0 mM $H_2O_2$ and 5.0 μM DAF-FM DA was studied (Fig. S4). Compared with Co-MOF, Co-FeMOF exhibits higher catalytic activity, suggesting Co in the MOF has not catalytic activity toward L-Arg oxidation, which is consistent with the result of ICP-OES (Table S2). To study the activity of GOD@Co-FeMOF, the kinetics and activity profile of the enzymatic reaction were studied (Fig. 2B and 2C). Compared with FeTCPP (Fig. 2B, curve a), Co-FeMOF (curve b) shows a higher catalytic rate, because FeTCPP as linker in Co-FeMOF avoided the formation of bridged μ-oxide dimers (hindered access to catalytic sites), intermolecular self-oxidation and oxidative self-degradation.[5b,25] After conjugation with GOD, the catalytic rate of GOD@Co-FeMOF (Fig. 2B, curve c) shows a slower catalytic rate than the Co-FeMOF, indicating GOD immobilized on nanosheets surface shields part of the catalytic sites. Based on GOD-catalyzed decomposition reaction of glucose, the result shows that the generated $H_2O_2$ concentrations quickly reach a plateau within only 30 min (Fig. S5A), suggesting the high catalytic efficiency of GOD. Fig. S5B shows GOD still keeps its activity after conjugating on the surface of Co-FeMOF, owing to the process of immobilizing is environmental friendly.[21c] After 30 min, the generated $H_2O_2$ concentrations reach a plateau.

The feasibility of the tandem catalysis was investigated by conducting the kinetics and activity profile of GOD@Co-FeMOF with DAF-FM DA probe at different conditions, and the results obtained were shown in Fig. 2C and 2D. With the time increasing, GOD@Co-FeMOF (Fig.2C, curve a), the mixture of GOD@Co-FeMOF and glucose (curve b) and the mixture of GOD@Co-FeMOF and L-Arg (curve c) show negligible fluorescence intensity changes, while the catalytic rate of the mixture of $H_2O_2$ and L-Arg increased (Fig.2D, curve a) with the time increasing. Comparing with the mixture of GOD, glucose and L-Arg (Fig.2D, curve b), the mixture of GOD@Co-FeMOF, glucose and L-Arg (curve c) shows a larger catalytic rate, which is consistent with the FL results (Fig. 2A). In this system, GOD@Co-FeMOF could oxidize glucose to yield $H_2O_2$, then the produced $H_2O_2$ could oxidize L-Arg to generate NO species and a byproduct of L-citrulline via the following two-steps (Fig. S6):

$$\text{Glucose} + O_2 \xrightarrow{\text{GOD}} \text{Gluconic acid} + H_2O_2 \quad (1)$$

$$\text{L-Arginine} + H_2O_2 \xrightarrow{\text{Co-FeMOF}} \text{L-Citrulline} + NO + H_2O \quad (2)$$

In order to further understand the impact of GOD@Co-FeMOF in the system, the kinetics and activity profile of GOD@Co-FeMOF with different concentration were studied (Fig. S7). The results show that the catalytic activity increases with the increasing of both the concentration of the GOD@Co-FeMOF and the reaction time, and reaches a plateau after the addition of 1.0 mg/mL GOD@Co-FeMOF. The impact of glucose concentrations in the system was measured by monitoring the time-dependent fluorescence intensity of benzotriazole derivative at 515 nm, which shows the catalytic activity increased with the glucose concentration increasing (Fig. S8) and the estimated $K_m$ of glucose is 4.6 mM according to the Lineweaver-Burk plot (Fig. S9). In the process, the generated $H_2O_2$ was measured by a $H_2O_2$ assay kit. The result shows that the generated $H_2O_2$ is increased in response to the elevated concentrations of glucose (Fig. 3A), because glucose oxidation could happen in the present of GOD. A kinetic study of the tandem catalytic reaction showed that the catalytic activity significantly increased with the increasing of L-Arg concentrations (Fig. S10) and the $K_m$ of L-Arg is 8.0 mM (Fig. S11). These results also suggest that the GOD@Co-FeMOF could catalyze L-Arg into NO in the presence of glucose, with the reaction orders of 0-1 with respect to either L-Arg or glucose.

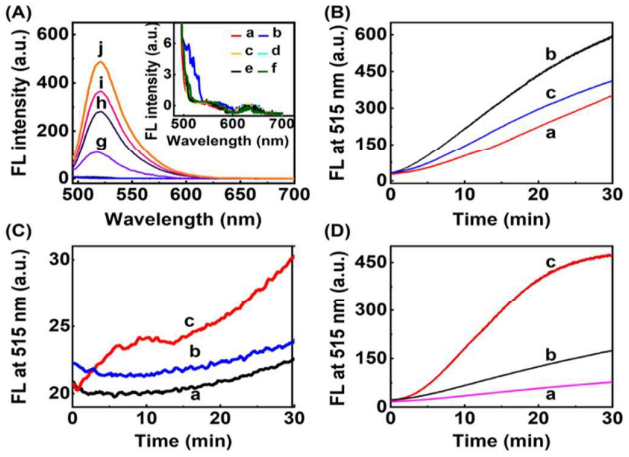


**Fig. 2** (A) FL of DAF-FM DA with Co-FeMOF (a), $H_2O_2$ (b), L-Arg (c), glucose (d), FeTCPP (e), GOD@Co-FeMOF (f), $H_2O_2$ + L-Arg (g), FeTCPP + $H_2O_2$ + L-Arg (h), GOD@Co-FeMOF + $H_2O_2$ + L-Arg (i) and Co-FeMOF + $H_2O_2$ + L-Arg (j). (B) Kinetic curves plotting the time-dependent fluorescence intensity at 515 nm for DAF-FM DA mixing with FeTCPP (a), Co-FeMOF (b) GOD@Co-FeMOF (c) at the present of $H_2O_2$ and L-Arg. Kinetic curves plotting the time-dependent fluorescence emission intensity at 515 nm for DAF-FM DA mixing with (C) GOD@Co-FeMOF (a), GOD@Co-FeMOF + glucose (b), GOD@Co-FeMOF + L-Arg (c) and (D) GOD + glucose + L-Arg (a), $H_2O_2$ + L-Arg (b) and GOD@Co-FeMOF + glucose + L-Arg (c). 5.0 mM $H_2O_2$, 20 mM L-Arg, 1.0 mg/mL glucose, 0.25 mg/mL FeTCPP, and 1.0 mg/mL GOD@Co-FeMOF. $E_x$=485 nm, $E_m$=515 nm.

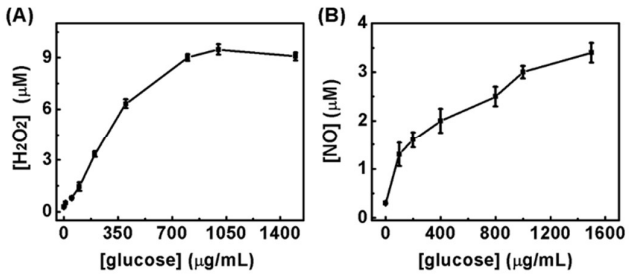


**Fig. 3** The generated (A) $H_2O_2$ concentration and (B) NO concentrations arising from the reaction between GOD@Co-FeMOF and different concentrations of glucose.

To study the generation of NO concentrations in the tandem catalytic reaction, the generated NO concentrations in solutions were measured using a typical Griess assay. Although the rate of the L-Arg-$H_2O_2$ reaction is slow in neutral solution,[19a] the generated NO increases with the increase of time and L-Arg concentration, and reaches the plateau with 20 mM L-Arg at 30 min in this catalytic system (Fig. S12). The reason for this phenomenon is that the generated gluconic acid could accelerate oxidization of L-Arg by

View Article Online
DOI: 10.1039/C8CC05068F




$H_2O_2$,[19a] in addition, the Co-FeMOF as the catalyst could increase the rate of reaction. As the concentration of glucose increases, the amount of generation NO increases (Fig. 3B). For the reaction, the generated NO amount depends on the produced $H_2O_2$ amount, and the latter relies on the added glucose concentration.

The stability of GOD@Co-FeMOF was measured by FL, XRD and SEM after five cycles in 0.1 M pH 6.9 and 7.4 PBS (Fig. S13-S17), which shows that the GOD@Co-FeMOF complex can maintain good and stable activity, and exhibits excellent catalysis.

In order to demonstrate that GOD@Co-FeMOF can function as effective catalysts for the generation of NO with endogenous components. The serum samples obtained from rabbit were properly diluted by 0.1 M PBS, and then mixed with the DAF-FM DA, GOD@Co-FeMOF and L-Arg. The result shows that NO is generated when GOD@Co-FeMOF is mixed with L-Arg and serum (Fig. S18), clearly indicating the approach could be used in complex sample to produce NO, and has the potential to use in biomedical field.

In summary, this work designs a simple, biocompatible and integrated tandem catalyst system based on conjugating GOD on Co-FeMOF. Co-FeMOF not only exhibits peroxidase-like activity but also could be as a support for the GOD immobilization. Besides, GOD@Co-FeMOF can drive a reaction cascade to allow for in situ generation of NO via the oxidation of L-Arginine in physiological pH. This process can thus allow the sustained generation of NO in the presence of glucose and L-Arginine, offering a potential solution to generate NO when in contact with serum. Overall, the Co-FeMOF bioassay described herein provides a general platform to integrate material catalysts with enzymatic catalysts for cascade reaction pathways under physiological pH, atmospheric pressure and aqueous solution conditions. Furthermore, this new method opens an avenue for designing biosensing strategies with multifunctional 2D MOFs, and can be used in synergistic starving-like/gas therapy. The next work is focused on reducing the size of 2D MOFs and employing in cancer therapy.

We gratefully acknowledge National Natural Science Foundation of China (21705004, 21675084), Natural Science Foundation of Anhui Province (1808085QB38) and Open Foundation of State Key Lab of Analytical Chemistry for Life Science, Nanjing University (SKLACLS1803).

## Conflicts of interest

There are no conflicts to declare.

## Notes and references

1 (a) H. T. T. Duong, N. N. M. Adnan, N. Barraud, J. S. Basuki, S. K. Kutty, K. Jung, N. Kumar, T. P. Davis and C. Boyer, *J. Mater. Chem. B*, 2014, **2**, 5003–5011; (b) A. de Mel, F. Murad and A. M. Seifalian, *Chem. Rev.*, 2011, **111**, 5742−5767.

2 (a) W. P. Fan, W. B. Bu, Z. Zhang, B. Shen, H. Zhang, Q. J. He, D. L. Ni, Z. W. Cui, K. L. Zhao, J. W. Bu, J. L. Du, J. N. Liu and J. L. Shi, *Angew. Chem. Int. Ed.*, 2015, **54**, 14026–14030; (b) H. J. Xiang, Q. Deng, L. An, M. Guo, S. P. Yang and J. G. Liu, *Chem. Commun.*, 2016, **52**, 148–151.

3 D. Hirst and T. Robson, *Curr. Pharm. Des.*, 2010, **16**, 411−420.

4 (a) R. M. J. Palmer, D. S. Ashton and S. Moncada, *Nature*, 1988, **333**, 664–666; (b) S. Kudo and Y. Nagasaki, *J. Controlled Release*, 2015, **217**, 256–262.

5 (a) F. Yang, P. Chen, W. He, N. Gu, X. Z. Zhang, K. Fang, Y. Zhang, J. F. Sun and J. Y. Tong, *Small*, 2010, **6**, 1300–1305; (b) M. Mukherjee and A. R. Ray, *Catal. Commun.*, 2007, **8**, 1431−1437. (c) M. Mukherjee, and A. R. Ray, *J. Mol. Catal. A Chem.*, 2007, **266**, 207–214.

6 R. Breslow and L. E. Overman, *J. Am. Chem. Soc.,* 1970, **92**, 1075–1077.

7 (a) R. Schlçgl, *Angew. Chem., Int. Ed.*, 2015, **54**, 3465−3520; (b) R. Ragg, M. N. Tahir and W. Tremel, *Eur. J. Inorg. Chem*., 2016, 1906–1915.

8 D. Wen, W. Liu, D. Haubold, C. Z. Zhu, M. Oschatz, M. Holzschuh, A. Wolf, F. Simon, S. Kaskel and A. Eychmuller, *ACS Nnao*, 2016, **10**, 2559-2567.

9 M. B. Gawande, A. Goswami, F. X. Felpin, T. Asefa, X. Huang, R. Silva, X. Zou, R. Zboril and R. S. Varma, *Chem. Rev*., 2016, **116**, 3722−3811.

10 (a) M. Vázquez-González, W. C. Liao, R. Cazelles, S. Wang, X. Yu, V. Gutkin and I. Willner, *ACS Nano*, 2017, **11**, 3247−3253; (b) S. Wang, R. Cazelles, W. C. Liao, M. Vázquez-González, A. Zoabi, R. Abu-Reziq and I. Willner, *Nano Lett.*, 2017, **17**, 2043–2048.

11 M. Vázquez-González, R. M. Torrente-Rodríguez, A. Kozell, W. C, Liao, A. Cecconello, S. Campuzano, J. M. Pingarron and I. Willner, *Nano Lett.*, 2017, **17**, 4958–4963.

12 B. W. Liu, Z. Y. Sun, P. J. J. Huang and J. W. Liu, *J. Am. Chem. Soc.*, 2015, **137**, 1290−1295.

13 I. I. Slowing, B. G. Trewyn and V. S. Y. Lin, *J. Am. Chem. Soc.*, 2007, **129**, 8845−8849.

14 G. Y. Tonga, Y. Jeong, B. Duncan, T. Mizuhara, R. Mout, R. Das, S. T. Kim, Y. C. Yeh, B. Yan, S. Hou and V. M. Rotello, *Nat. Chem.*, 2015, **7**, 597−603.

15 Y. Zhang, Z. Y. Wang, X. J. Li, L. Wang, M. Yin, L. H. Wang, N. Chen, C. H. Fan and H. Y. Song, *Adv. Mater.*, 2016, **28**, 1387−1393.

16 (a) A. C. Marr and S. Liu, *Trends Biotechnol.*, 2011, **29**, 199–204; (b) Q. Q. Wang, X. P. Zhang, L. Huang, Z. Q. Zhang, and S. J. Dong, *Angew. Chem., Int. Ed.*, 2017, **56**, 1−3.

17 (a) S. Hudson, J. Cooney and E. Magner, *Angew. Chem., Int. Ed.*, 2008, **47**, 8582−8594; (b) M. Hartmann, *Chem. Mater.*, 2005, **17**, 4577−4593; (c) Z. Li and K. S. Suslick, *ACS Appl. Mater. Interfaces*, 2018, **10**, 15820−15828; (d) Z. Li and K. S. Suslick, *ACS Sens*., 2018, **3**, 121−127.

18 M. Hartmann and D. J. Jung, *J. Mater. Chem.*, 2010, **20**, 844–857.

19 (a) W. P. Fan, N. Lu, P. Huang, Y. Liu, Z. Yang, S. Wang, G. C. Yu, Y. J. Liu, J. K. Hu, Q. J. He, J. l. Qu, T. F. Wang and X. Y. Chen, *Angew. Chem. Int. Ed.*, 2016, **55**, 1–6; (b) Q. Sun, C. W. Fu, B. Aguila, J. Perman, S. Wang, H. Y. Huang, F. S. Xiao and S. Q, Ma, *J. Am. Chem. Soc.*, 2018, **140**, 984−992.

20 (a) Y. Peng, Y. S. Li, Y. J. Ban, H. Jin, W. M. Jiao, X. L. Liu and W. S. Yang, *Science*, 2014, **346**, 1356–1359; (b) T. Rodenas, I. Luz, G. Prieto, B. Seoane, H. Miro, A. Corma, F. Kapteijn, F. X. Llabrési Xamena and J. Gascon, *Nat. Mater.*, 2015, **14**, 48–55. (c) M. T. Zhao, Y. X. Wang, Q. L. Ma, Y. Huang, X. Zhang, J. F. Ping, Z. C. Zhang, Q. P. Lu, Y. F. Yu, H. Xu, Y. L. Zhao and H. Zhang, *Adv. Mat*., 2015, **27**, 7372–7378.

21 (a) Y. X. Wang, M. T. Zhao, J. F. Ping, B. Chen, X. H. Cao, Y. Huang, C. L. Tan, Q. L. Ma, S. X. Wu, Y. F. Yu, Q. P. Lu, J. Z. Chen, W. Zhao, Y. B. Ying and H. Zhang, *Adv. Mater*., 2016, **28**, 4149–4155; (b) M. Xu, S. Yuan, X. Y. Chen, Y. J. Chang, G. Day, Z. Y. Gu and H. C. Zhou, *J. Am. Chem. Soc.*, 2017, **139**, 8312−8319.

22 L. Y. Cao, Z. K. Lin, F. Peng, W. W. Wang, R. Y. Huang, C. Wang, J. W. Yan, J. Liang, Z. M. Zhang, T. Zhang, L. S. Long, J. L. Sun and W. B. Lin, *Angew. Chem., Int. Ed.*, 2016, **55**, 4962–4966.

23 R. W. Larsen, J. Miksovska, R. L. Musselman and L. J. Wojtas, *Phys. Chem. A*, 2011, **115**, 11519−11524.

24 M. G. Espey, K. M. Miranda, D. D. Thomas and D. A. Wink, *Free Radical Biol. Med*., 2002, **33**, 827–834.

25 S. E. J. Bell, R. E. Hester, J. N. Hill, D. R. Shawcross and J. R. L Smith, *J. Chem. Soc., Faraday Trans.*, 1990, **86**, 4017−4023.

View Article Online
DOI: 10.1039/C8CC05068F



Graphical Abstract:

# Enzyme-immobilized metal-organic framework nanosheets as tandem catalysts for generation of nitric oxide

By Pinghua Ling,[a*] Caihua qian,[a] Feng Gao[a] and Jianping Lei[b]*

**An enzyme-immobilized metal-organic framework nanosystem was developed as a tandem catalyst for in-situ generation of nitric oxide in serum samples.**